Image Cover Sheet

IEEE TRANSACTIONS ON IMAGE PROCESSING, VOL. 4, NO. 4, APRIL 1995

A Comparison of Rotational Representations in Structure and Motion Estimation for Maneuvering Objects

Victor C. Aitken and Howard M. Schwartz

Abstract— **Alternative methods are examined for estimating motion and structure of objects undergoing smooth maneuvers through measurements of feature positions in long, multiple-camera image sequences. Performance of extended Kalman filters are compared for Euler angle-axis, roll-pitch-yaw, and quaternion parameterizations of rotational motion. The angle-axis method was found to give the best overall performance with a computationally efficient implementation.**

I. Introduction

Estimation of rotational motion is an integral component of the object tracking problem. Selection of a parameterization for rotational motion, therefore, is an important aspect in the design of tracking algorithms in order to achieve an acceptable balance between possibly conflicting requirements of efficiency and accuracy. Two examples are unit quaternions [1]–[3], for which dynamical models are nonlinear and estimation is subject to a nonlinear constraint, and Euler angles, which may be poorly behaved numerically [1] and have led to computationally demanding implementations [4]. Moreover, many existing methods, [1]–[4] for example, may yield unsatisfactory performance for maneuvering objects since structural models have strict dependence on assumptions concerning the nature of translational and/or rotational motion. We have addressed these issues in recent research [7] and summarize our methods and results in this correspondence. Motion, structure, and measurement models are developed for a rigid maneuvering object observed with a multiple-camera imaging system. Estimation performance of extended Kalman filters based on Euler angle-axis, roll-pitch-yaw, and quaternion parameterizations are compared for maneuvering object trajectories.

Manuscript received June 12, 1993; revised January 19, 1994. The associate editor coordinating the review of this paper and approving it for publication was Dr. Homer H. Chen.
V. C. Aitken is with the Defence Research Establishment Suffield, Medicine Hat, T1A 8K6 Canada.
H. M. Schwartz is with the Department of Systems and Computer Engineering, Carleton University, Ottawa, K1S 5B6 Canada.
IEEE Log Number 9409285.

II. Structure, Translational Motion, and Measurement Models

Two or more cameras observe a rigid object whose motion is both translational and rotational. Multiple reference frames, denoted as $F_O \sim$ object-fixed, $F_E \sim$ earth-fixed, and $F_{C_j} \sim j$th camera-fixed, $j = 1, \ldots, N_C$, for N_C-ocular imaging systems, are defined. A vector $\mathbf{r}$ expressed with respect to F_α, $\alpha \in \{O, E, C_j\}$, with origin O_α, is denoted by $\mathbf{r}_\alpha = [r_{\alpha,1}, r_{\alpha,2}, r_{\alpha,3}]_\alpha^T$. A second reference frame F_β is related to F_α by a translation $\mathbf{T}_\beta^\alpha$ from O_α to O_β and a rotation from the α-basis to the β-basis $\mathbf{I}_\beta^\alpha$, and we write $[\mathbf{r}_\alpha]_\beta := \mathbf{I}_\beta^\alpha \mathbf{r}_\alpha$ and $\mathbf{r}_\beta = [\mathbf{r}_\alpha]_\beta + [\mathbf{T}_\alpha^\beta]_\beta$. The position $[\mathbf{T}_{C_j}^E]_E$ and orientation $\mathbf{I}_{C_j}^E$ of the jth camera frame F_{C_j} is known or estimated with respect to F_E. The overall state vector is $\mathbf{x} = [\mathbf{x}_t^T, \mathbf{x}_r^T, \mathbf{x}_s^T]^T$, where $\mathbf{x}_t$, $\mathbf{x}_r$, and $\mathbf{x}_s$ are the translational motion, rotational motion, and structure state vectors, respectively.

A. Structure Model

The constant structure state vector for N_f observed feature points contains position vectors $\mathbf{r}_O^i$ and is written as $\mathbf{x}_s = [(\mathbf{r}_O^1)^T, \ldots, (\mathbf{r}_O^{N_f})^T]^T$. The object-centered frame is fixed on the object by selecting from $\mathbf{x}_s$ three noncollinear feature points $\{p^1, p^2, p^3\}$ and imposing the following constraints: 1) in F_O, p^1 lies at a known position $\mathbf{d}_O = [d_{O,1}, d_{O,2}, d_{O,3}]^T$, which is fixed at the time of filter initialization and thereafter remains constant [7], and hence, its structure vector is known; 2) the x-axis of F_O is parallel to the line passing through p^1 and p^2 so that the y_O- and z_O-coordinates of the structure vector of p^2 are known to be $d_{O,2}$ and $d_{O,3}$, respectively; and 3) the x-y coordinate plane of F_O is parallel to the plane containing p^1, p^2, and p^3 so that the z_O-coordinate of the structure vector of the p^3 is known to be $d_{O,3}$. These constraints are enforced by treating the six known structural coordinates as known parameters in the estimation process. This method results in one of four possible orientations of F_O with respect to the three points; the distinct solutions are related by rotations of the basis set by 0 or π about a coordinate axis. The important advantage, however, is that F_O is defined independent of object motion.

B. Translational Motion

The position of the object-centered frame $\mathbf{p}(t) := [\mathbf{T}_O^E]_E(t)$ and its first N_p time derivatives form the translational motion state vector $\mathbf{x}_t$, which is written as $\mathbf{x}_t = [\mathbf{p}^T, \dot{\mathbf{p}}^T, \ldots, (\partial^{N_p}\mathbf{p}/\partial t^{N_p})^T]^T$. Singer's approach [6] for maneuvering objects is employed, in which the highest time derivatives in the state vector are modeled as first-order Gauss-Markov processes with variance σ_t^2 and reciprocal maneuver correlation time constant α_t. In this case, $\mathbf{x}_t$ propagates in time according to $\dot{\mathbf{x}}_t(t) = \mathbf{A}_t\mathbf{x}_t(t) + \mathbf{G}_t\mathbf{w}_t(t)$, where

$$\mathbf{A}_t = \begin{bmatrix} \mathbf{0}_{3N_p\times 3} & \mathbf{I}_{3N_p} \\ \mathbf{0}_{3\times 3N_p} & -\alpha_t\mathbf{I}_3 \end{bmatrix}, \quad \mathbf{G}_t = \begin{bmatrix} \mathbf{0}_{3N_p\times 3} \\ \mathbf{I}_3 \end{bmatrix} \tag{1}$$

$\mathbf{w}_t(t)$ is zero-mean, white Gaussian noise with covariance $\mathbf{Q}_t = 2\alpha_t\sigma_t^2\mathbf{I}_3$, and $\mathbf{I}_n$ denotes the $n \times n$ identity matrix, while $\mathbf{0}_{n\times m}$ is an $n \times m$ matrix of zeros. Singer [6] has proposed methods for selection of α_t and σ_t, which can be treated as tuning parameters in the filtering equations, while selection of N_p would generally depend on the expected complexity of object motion.

C. Measurement Model

The position of the ith feature point with respect to F_{C_j} is given by $\mathbf{r}_{C_j}^i = \mathbf{I}_{C_j}^E\{\mathbf{I}_E^O\mathbf{r}_O^i + [\mathbf{T}_O^E]_E\} - [\mathbf{T}_{C_j}^E]_{C_j}$. The measurement model for the jth camera is then written as $\mathbf{z}_j(k) = \mathbf{h}_j[\mathbf{x}(k)] + \mathbf{v}_j(k)$, where $\mathbf{h}_j[\mathbf{x}(k)] := [\mathbf{h}_j^1[\mathbf{x}(k)]^T, \ldots, \mathbf{h}_j^{N_f}[\mathbf{x}(k)]^T]^T$, $\mathbf{v}_j(k)$ represents measurement noise, and the image plane position $\mathbf{h}_j^i[\mathbf{x}(k)]$ of the ith feature point in the jth camera is computed through perspective projection, with L_j representing the effective focal length of the jth camera as $\mathbf{h}_j^i[\mathbf{x}(k)] = L_j[r_{C_j,2}^i, r_{C_j,3}^i]^T/r_{C_j,1}^i$. The overall measurement model is written as $\mathbf{z}(k) = \mathbf{h}[\mathbf{x}(k)] + \mathbf{v}(k)$, where $\mathbf{z} = [\mathbf{z}_1^T, \ldots, \mathbf{z}_{N_C}^T]^T$, $\mathbf{h} = [\mathbf{h}_1^T, \ldots, \mathbf{h}_{N_C}^T]^T$, and $\mathbf{v} = [\mathbf{v}_1^T, \ldots, \mathbf{v}_{N_C}^T]^T$.

III. Rotational Motion

The object's instantaneous orientation $\mathbf{I}_E^O(\boldsymbol{\zeta})$ depends on the parameterization $\boldsymbol{\zeta}$ selected for rotational motion. The angle-axis and roll-pitch-yaw parameterizations result in simple approximate linear dynamic models, whereas the quaternion formulation results in a more complex but still approximate nonlinear model.

A. Angle-Axis Parameterization

Rotational motion is modeled by the temporal behavior of an orientation vector $\boldsymbol{\xi} = [\xi_1, \xi_2, \xi_3]^T$, whose direction $\bar{\boldsymbol{\xi}} := \boldsymbol{\xi}/\|\boldsymbol{\xi}\|$ specifies the axis of the rotation relating F_E and F_O, and whose magnitude $\gamma := \|\boldsymbol{\xi}\|$ specifies the angle of rotation about $\bar{\boldsymbol{\xi}}$. In this case, $\mathbf{I}_E^O(\boldsymbol{\xi}) = \exp(\boldsymbol{\xi}^\sharp) = \mathbf{I}_3 + \sin(\gamma)\bar{\boldsymbol{\xi}}^\sharp + [1 - \cos(\gamma)](\bar{\boldsymbol{\xi}}^\sharp)^2$, where the matrix cross product operator $(\cdot)^\sharp$ is defined as

$$\boldsymbol{\xi}^\sharp := \begin{bmatrix} 0 & -\xi_3 & \xi_2 \\ \xi_3 & 0 & -\xi_1 \\ -\xi_2 & \xi_1 & 0 \end{bmatrix}. \tag{2}$$

The rotational motion state vector $\mathbf{x}_r$ is constructed from $\boldsymbol{\xi}$and its first N_ξ time derivatives, and approximate temporal behavior is again modeled with Singer's method, as was done for translational motion, but with parameters α_r and σ_r^2. The instantaneous angular velocity ω of F_O with respect to F_E expressed in F_E, if required, is computed from the state estimate as $\omega = \dot{\gamma}\bar{\boldsymbol{\xi}} + \sin(\gamma)\dot{\bar{\boldsymbol{\xi}}} + [1 - \cos(\gamma)]\bar{\boldsymbol{\xi}}^\sharp\dot{\bar{\boldsymbol{\xi}}}$.

Occasionally, the orientation vector $\boldsymbol{\xi}$ must be reset, first to maintain a finite magnitude (rotation angle) and second to yield decreasing Cramer-Rao bounds [7]. A trajectory $\boldsymbol{\xi}(t)$ in the region $\pi < \|\boldsymbol{\xi}\| < 2\pi$ is equivalent, in the sense that it produces the same rotation matrix, to a trajectory $\boldsymbol{\zeta}(t)$ in the region $\|\boldsymbol{\zeta}\| < \pi$ if $\boldsymbol{\zeta}(t) = \boldsymbol{\xi}(t) - 2\pi\bar{\boldsymbol{\xi}}(t)$, which leads to an approximate impulsive reset for $\boldsymbol{\xi}$ and its time derivatives to enforce $\gamma \in [0, \pi]$.

B. Roll-Pitch-Yaw Parameterization

The roll (ϕ), pitch (θ), and yaw (ψ) angles define an ordered sequence of three plane rotations $\mathbf{I}_E^O = \exp(\psi\mathbf{e}_3^\sharp)\exp(\theta\mathbf{e}_2^\sharp)\exp(\phi\mathbf{e}_1^\sharp)$, where $\mathbf{e}_i$, $i = 1, 2, 3$ are the standard basis vectors of $\mathbb{R}^3$. In this case, the parameter vector is defined as $\boldsymbol{\zeta} := [\phi, \theta, \psi]^T$. The rotational motion state vector $\mathbf{x}_r$ is constructed from $\boldsymbol{\zeta}$ and its first N_ζ time derivatives, and approximate temporal behavior is again modeled with Singer's method, as was done for translational motion, but with parameters α_r and σ_r^2. Angular velocity, if required, is computed from the state estimate as $\omega = \mathbf{J}_{rpy} * [\dot{\phi}, \dot{\theta}, \dot{\psi}]^T$, where

$$\mathbf{J}_{rpy} := \begin{bmatrix} \cos(\psi)\cos(\theta) & -\sin(\psi) & 0 \\ \sin(\psi)\cos(\theta) & \cos(\psi) & 0 \\ -\sin(\theta) & 0 & 1 \end{bmatrix}. \tag{3}$$

The matrix $\mathbf{J}_{rpy}$ is singular for $\theta = \pm\pi/2$. A simple calculation shows that at these orientations, any nonzero component of angular velocity in span$\{\cos(\psi), \sin(\psi), 0]^T\}$ cannot be representated by this parameterization with finite $\dot{\phi}$, $\dot{\theta}$, and $\dot{\psi}$. Computing ω from the state estimate in this manner can, therefore, lead to significant errors about the singular orientations $\theta = \pm\pi/2$.

C. Quaternion Parameterization

With $\bar{\boldsymbol{\xi}}$ and γ defined as in the angle-axis parameterization, the unit quaternion [1]–[3], [5], [8] defined by $\bar{\mathbf{q}} := \mathbf{q}/\|\mathbf{q}\| := [-\bar{\boldsymbol{\xi}}^T\sin(\gamma/2), \cos(\gamma/2)]^T$ gives $\mathbf{I}_E^O(\mathbf{q}) = (1/\|\mathbf{q}\|^2)\mathbf{\Gamma}(\mathbf{q}) = \mathbf{\Gamma}(\bar{\mathbf{q}})$, where

$$\mathbf{\Gamma}(\mathbf{q}) := \begin{bmatrix} q_1^2 - q_2^2 - q_3^2 + q_4^2 & 2(q_1q_2 + q_3q_4) & 2(q_1q_3 - q_2q_4) \\ 2(q_1q_2 - q_3q_4) & -q_1^2 + q_2^2 - q_3^2 + q_4^2 & 2(q_2q_3 + q_1q_4) \\ 2(q_1q_3 + q_2q_4) & 2(q_2q_3 - q_1q_4) & -q_1^2 - q_2^2 + q_3^2 + q_4^2 \end{bmatrix}. \tag{4}$$

The matrix $\mathbf{\Gamma}(\mathbf{q})$ represents combined operations of rotation about $\bar{\boldsymbol{\xi}}$ by the angle γ as well as scaling by $\|\mathbf{q}\|^2$.

Temporal dependence of the quaternion on angular velocity is given by $\dot{\mathbf{q}}(t) = \mathbf{\Omega}[\omega(t)]\mathbf{q}(t)$, where

$$\mathbf{\Omega}[\omega] := \frac{1}{2}\begin{bmatrix} \omega^{\xi} & -\omega \\ \omega^T & 0 \end{bmatrix}. \tag{5}$$

A state vector $\mathbf{x}_\omega$ for the angular velocity and its first N_ω time derivatives is defined in a manner equivalent to that employed for translational motion, but with parameters $\mathbf{A}_\omega$, $\mathbf{G}_\omega$, α_r, and σ_r^2. An overall state vector $\mathbf{x}_r$ corresponding to rotational motion is defined as $\mathbf{x}_r := \left[\mathbf{q}^T, \mathbf{x}_\omega^T\right]^T$, which propagates in time according to the nonlinear differential equation

$$\dot{\mathbf{x}}_r(t) = \begin{bmatrix} \mathbf{\Omega}[\omega(t)] & \mathbf{0} \\ \mathbf{0} & \mathbf{A}_\omega \end{bmatrix}\mathbf{x}_r(t) + \begin{bmatrix} \mathbf{0}_{4\times 3} \\ \mathbf{G}_\omega \end{bmatrix}\mathbf{w}_r(t). \tag{6}$$

Time propagation in the extended Kalman filter requires numerical integration of (6) without the noise term. Moreover, because $\mathbf{\Omega}$ is skew-symmetric, $\mathbf{q}^T\dot{\mathbf{q}} = 0$, which dictates that time propagation in the filter should maintain constant quaternion norm. We assume that the highest time derivative of ω in $\mathbf{x}_\omega$ is approximately constant over any sample period and employ an algorithm that is similar in form to one analyzed by Branets and Shmyglevski [8]. Define a partition $\{t_k = \tau_0 \leq \tau_1 \leq \cdots \leq \tau_{N_\pi} = t_{k+1}\}$ of the kth sample period and assume for convenience that $\tau_{\ell+1} - \tau_\ell \equiv \tau$ is constant. With the linear model for $\mathbf{x}_\omega$, $\mathbf{x}_\omega(\tau_\ell) = [\mathbf{\Phi}_\omega(\tau)]^\ell\mathbf{x}_\omega(t_k)$ and $\omega(\tau_\ell) = \mathbf{C}_\omega\mathbf{x}_\omega(\tau_\ell)$, where $\mathbf{\Phi}_\omega(\tau) := \exp\{\mathbf{A}_\omega\tau\}$ and $\mathbf{C}_\omega := [\mathbf{I}_3, \mathbf{0}_{3\times N_\omega}]$. Time propagation of $\mathbf{q}$, while maintaining $\|\mathbf{q}(k+1)\| = \|\mathbf{q}(k)\|$, over any sample period may be approximated by $\mathbf{q}(k+1) = \mathbf{\Phi}_q(k)\mathbf{q}(k)$, where

$$\mathbf{\Phi}_q(k) := \downarrow\prod_{\ell=0}^{N_\pi-1}\exp\left\{\mathbf{\Omega}\left[\mathbf{C}_\omega(\mathbf{\Phi}_\omega(\tau))^\ell\mathbf{x}_\omega(t_k)\right]\tau\right\} \tag{7}$$

in which "$\downarrow\prod$" indicates that the index ℓ decreases from left to right in the matrix product $\mathbf{\Omega}[\cdot] : \mathbb{R}^3 \to \mathbb{R}^{4\times 4}$ according to (5), and the matrix exponentials can be evaluated with $\exp\{\mathbf{\Omega}[\omega]\tau\} = 2\sin(\|\omega\|\tau/2)\mathbf{\Omega}[\omega]/\|\omega\| + \cos(\|\omega\|\tau/2)\mathbf{I}_4$. Time propagation of $\mathbf{x}_r$ is then computed as $\mathbf{x}_r(k+1) = \mathbf{\Phi}_r(k)\mathbf{x}_r(k)$, where $\mathbf{\Phi}_r(k) := \mathrm{diag}\{\mathbf{\Phi}_q(k), \mathbf{\Phi}_\omega(T)\}$, with T being the sample period.

However, the block diagonal matrix $\mathbf{\Phi}_r(k)$ cannot be used in an overall block diagonal state transition matrix to propagate the Kalman covariance matrix over time since this would imply no temporal dependence of the quaternions on angular velocity. Instead, approximate time propagation [1]–[3] of the covariance matrix is performed with an approximate state transition matrix in which the rotational motion component is $\hat{\mathbf{\Phi}}_r(k) := \exp\{\mathbf{F}_r(k)T\}$, where $\mathbf{F}_r(k)$ is the Jacobian, with respect to $\mathbf{x}_r$, of (6) without the noise term.

The primary difficulty with the quaternion approach is that the desired nonlinear constraint $\|\mathbf{q}\| = 1$ is not easily incorporated into the linear form of the measurement update in the Kalman filtering equations. A common approach [1]–[3] of applying an impulsive normalization of the estimated quaternion $\hat{\mathbf{q}}(k|k) \leftarrow \hat{\mathbf{q}}(k|k)/\|\hat{\mathbf{q}}(k|k)\|$ immediately following each observation event is an outside intervention in the filtering process, which, if applied alone, has not been analyzed. In fact, we have found in simulations [7] that this approach in the present problem led to very poor and often divergent behavior of the extended Kalman filter. Bar-Itzhack and Oshman [5] extracted a unit quaternion with a similar approach and used a linear analysis to conclude that this reset operation can be applied for output purposes *provided* that the portion of the estimated quaternion that is lost due to normalization is propagated in the filter. Following the main ideas of this approach, we propagate the entire quaternion estimate in the filter and, for output purposes only, extract a normalized quaternion and appropriately scaled structure estimates.

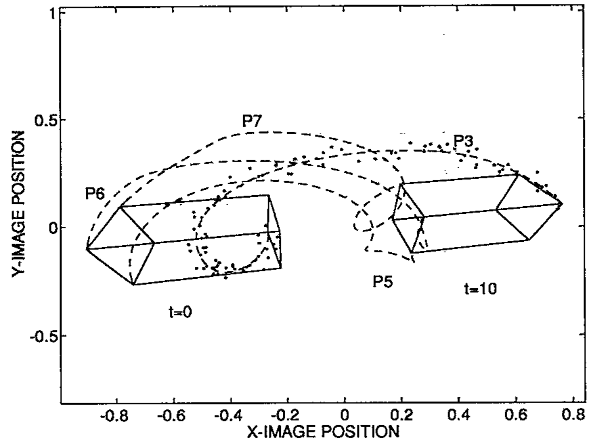

Fig. 1. Image plane trajectories of feature points used in simulation. Sample measurement noise is overlaid on P3 trajectory.

The quaternion-based filter has been implemented [7] with the following approach: 1) $\|\hat{\mathbf{q}}(0|-1)\| = 1$; 2) $\|\hat{\mathbf{q}}(k+1|k)\| = \|\hat{\mathbf{q}}(k|k)\|$; 3) the measurement model employs $\mathbf{\Gamma}(\hat{\mathbf{q}})$ of (4) as the transformation from F_O to F_E; 4) for output purposes only, the estimated unit quaternion is taken as $\bar{\hat{\mathbf{q}}}(k|k) := \hat{\mathbf{q}}(k|k)/\|\hat{\mathbf{q}}(k|k)\|$, and, again for output purposes only, structure estimates denoted ${}^*\hat{\mathbf{r}}_O^i(k|k)$ are taken as ${}^*\hat{\mathbf{r}}_O^i(k|k) := \|\hat{\mathbf{q}}(k|k)\|^2\hat{\mathbf{r}}_O^i(k|k)$, where the vectors $\hat{\mathbf{r}}_O^i(k|k)$ are structure estimates generated within the filter; and 5) in the kth measurement update, $\hat{\mathbf{d}}_0 := \mathbf{d}_0/\|\mathbf{q}(k|k-1)\|^2$ is used in place of $\mathbf{d}_0$ within the filter.

In step 3), above, the use of $\mathbf{\Gamma}(\hat{\mathbf{q}})$ means that all structure estimates within the filter $\hat{\mathbf{r}}_O^i$ are scaled by $\|\hat{\mathbf{q}}\|^2$ in the transformation from F_O to F_E. The result of step 4) is that structural estimates, when referenced to the earth-fixed frame within the filter, exactly match those extracted from the filter for output purposes: $\mathbf{\Gamma}(\hat{\mathbf{q}}(k|k))\hat{\mathbf{r}}_O^i(k|k) = \mathbf{I}_E^O(\bar{\hat{\mathbf{q}}}(k|k))[{}^*\hat{\mathbf{r}}_O^i(k|k)]$. However, two problems arise from the inability to enforce the constraint $\|\hat{\mathbf{q}}\| = 1$ throughout the measurement update. First, structure estimation errors in the output are computed from $\mathbf{r}_O^i - \|\hat{\mathbf{q}}(k|k)\|^2\hat{\mathbf{r}}_O^i(k|k)$, which demonstrates an extra degree of freedom in the filter that can result in a reduced rate of accumulation of information concerning object structure. This difficulty has been demonstrated through Cramer-Rao bound analysis [7]. The second problem is that structural constraints based on the known vector $\mathbf{d}_O$, which defines the position and orientation of F_O with respect to three observed feature points, are not maintained throughout the measurement update. On entry to the measurement update equations, these constraints are satisfied in the sense that $\mathbf{\Gamma}(\hat{\mathbf{q}}(k|k-1))\hat{\mathbf{d}}_0 = \mathbf{I}_E^O(\hat{\mathbf{q}}(k|k-1))\mathbf{d}_O$. However, because the quaternion norm is not generally invariant over the measurement update, these constraints may not be precisely satisfied on exit from the measurement update equations; on exit $\mathbf{\Gamma}(\hat{\mathbf{q}}(k|k))\hat{\mathbf{d}}_0 = \mathbf{I}_E^O(\hat{\mathbf{q}}(k|k))\mathbf{d}_O\{\|\mathbf{q}(k|k)\|^2/\|\mathbf{q}(k|k-1)\|^2\}$. This inherent scaling of the structural constraints by $\|\mathbf{q}(k|k)\|^2/\|\mathbf{q}(k|k-1)\|^2$ over the measurement update can effect structure estimates as well as position and translational motion estimates.

IV. Example Simulation Results

Extended Kalman filters for each of the above parameterizations were implemented with local iterations at each observation event and a simple single-frame initialization [7] of position, orientation, and structure, while all temporal derivatives were initialized at zero. Simulations with synthetic imagery generally were consistent with the previous discussions in that the roll-pitch-yaw-based filter

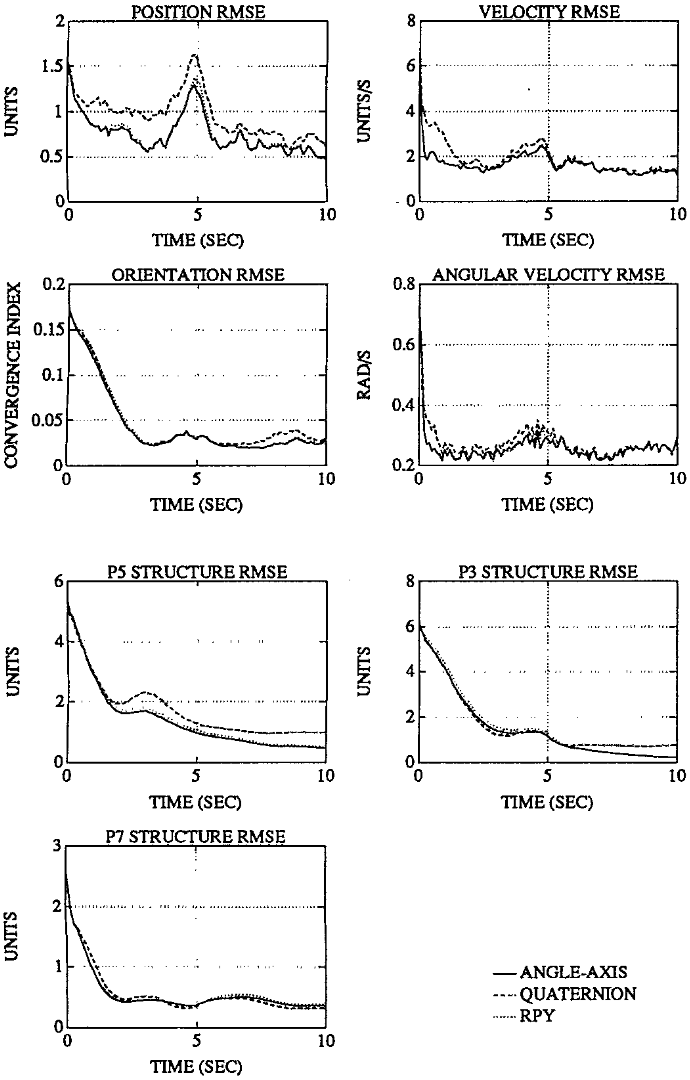

Fig. 2. Comparison of Monte Carlo simulation results for the angle-axis, roll-pitch-yaw, and quaternion filters.

sometimes gave poor results in angular velocity estimates about $\theta = \pm\pi/2$, while the quaternion-based filter showed poorer performance in estimation of position and some structural parameters. Fig. 1 illustrates four feature point trajectories in one camera of a binocular stereo pair for sinusoidal roll, pitch, and yaw angles and constant acceleration of the centroid (not coincident with the origin of F_O) of a rectangular block. Special feature points of the structural model were selected as $p^1 = P6$, $p^2 = P3$, and $p^3 = P7$, with $P5$ unknown (six unknown structural parameters in total). Sample measurement noise is overlaid on the $P3$ trajectory. Model parameters are taken as $N_f = 4$, $N_t = 2$, $\alpha_t = 0.5$, $\sigma_t = 8$, $N_\xi = N_\zeta = 2$, $N_\omega = 1$, and $N_\pi = 5$, with $\alpha_r = 0.5$ and $\sigma_r = 4$ for all three filters. The sample period is $T = 0.1$ s, and uniformly distributed measurement errors of 5 to 10% of the object image size were assumed. Fig. 2 shows root-mean-square errors over 60 runs of the Euclidean norm of position, velocity, angular velocity, and structure errors and of the Frobenius norm, scaled so that the maximum value is 1, of the difference between true and estimated rotation matrices. The roll-pitch-yaw (dotted traces) and angle-axis (solid traces) filters show very similar performance for this trajectory, with improvements over the quaternion filter (dashed traces) in position and some structure estimation.

TABLE I
TIME INTERVAL TEST OF MEANS FOR COMPARISON OF ANGLE-AXIS AND QUATERNION ALGORITHMS: TEST VALUES GREATER THAN 1.65 INFER SUPERIOR PERFORMANCE OF THE ANGLE-AXIS ALGORITHM OVER THE QUATERNION ALGORITHM AT THE 95% CONFIDENCE LEVEL FOR THE INDICATED TIME INTERVAL OF THE TRAJECTORY SHOWN IN FIG. 1

TIME INT.	0-20	20-40	40-60	60-80	80-100
POSITION	4.90	5.13	4.60	4.62	4.21
ORIENTATION	1.40	0.63	0.42	3.62	6.12
ANG. VEL.	5.53	12.57	8.35	15.07	0.70
P5 STRUCTURE	0.54	3.51	6.72	6.66	8.01

Bar-Shalom and Fortmann [9] describe in detail a procedure for statistical comparison of algorithm performance that can be applied, assuming that the sum of estimation errors at each time update over the 60 runs exhibits approximately normal statistics. Using this method, Table I shows the test statistics for which values greater than 1.65 infer superior performance of the angle-axis algorithm over the quaternion algorithm at the 95% confidence level for the indicated time interval of the trajectory shown in Fig. 1. Statistically significant improvements of the angle-axis approach over the quaternion approach are observed in position over all time intervals, in orientation from 60 s to the end of the run, in angular velocity from initialization to 80 s, and in $P5$-structure from 20 s to the end of the run.

V. CONCLUSIONS

This work not only demonstrates how previously proposed quaternion-based approaches, in which structural models were strictly dependent on motion assumptions, might be extended to track maneuvering objects observed in multiple-camera image sequences, but also provides two much simpler alternatives using angle-axis and roll-pitch-yaw parameterizations. The roll-pitch-yaw approach, however, can lead to poor performance in angular velocity estimation at particular orientations. The quaternion-based filter suffers from an extra degree of freedom arising from the inability to impose a constraint of constant quaternion norm throughout the measurement update, which can degrade estimates of translational motion and structure. The angle-axis filter, based on a simple linear dynamical model, was found to give the best overall performance with reduced computational requirements in comparison to the quaternion filter.

REFERENCES

[1] T. Broida, S. Chandrashekhar, and R. Chellappa, "Recursive 3-D motion estimation from a monocular image sequence," *IEEE Trans. Aerosp. Electron. Syst.*, vol. 26, no. 4, pp. 639–656, July 1990.
[2] G. J. Young and R. Chellappa, "3-D motion estimation using a sequence of noisy stereo images: models, estimation, and uniqueness results," *IEEE Trans. Pattern Anal. Machine Intell.*, vol. 12, no. 8, pp. 735–759, Aug. 1990.
[3] T. J. Broida and R. Chellappa, "Estimating the kinematics and structure of a rigid object from a sequence of monocular images," *IEEE Trans. Pattern Anal. Machine Intell.*, vol. 13, no. 6, pp. 497–513, 1991.
[4] J. J. Wu, R. E. Rink, T. M. Caelli, and V. G. Gourishankar, "Recovery of the 3-D location and motion of a rigid object through camera image (an extended Kalman filter approach)," *Int. J. Comput. Vis.*, vol. 2, no. 4, pp. 373–394, 1989.
[5] I. Y. Bar-Itzhack and Y. Oshman, "Attitude determination from vector observations: quaternion estimation," *IEEE Trans. Aerosp. Electron. Syst.*, vol. AES-21, no. 1, pp. 128–135, Jan. 1985.
[6] R. A. Singer, "Estimating optimal tracking filter performance for manned maneuvering targets," *IEEE Trans. Aerosp. Electron. Syst.*, vol. AES-6, no. 4, pp. 473–483, July 1970.
[7] V. C. Aitken, "Motion and structure estimation of maneuvering objects in multiple-camera image sequences," Defence Research Establishment Suffield, Medicine Hat, Alberta, Canada, Suffield Report no. SR-577, 1992.

[8] V. N. Branets and I. P. Shmyglevski, *Application of Quaternions to Rigid Body Rotation Problems*. Moscow: Nauka, 1973; NASA technical translation NASA TT F-15,414, translated for NASA under contract no. NASw 2483 by SCITRAN, Santa Barbara, CA.
[9] Y. Bar-Shalom and T. E. Fortmann, *Tracking and Data Association*, London: Academic, 1988, Appendix B and pp. 145–148.

151454

NO. OF COPIES NOMBRE DE COPIES	COPY NO. COPIE N°	INFORMATION SCIENTIST'S INITIALS INITIALES DE L'AGENT D'INFORMATION SCIENTIFIQUE
1	1	DAG
AQUISITION ROUTE FOURNI PAR ▶	DRES	
DATE ▶	09 May 91	
DSIS ACCESSION NO. NUMÉRO DSIS ▶		

DND 1158 (6-87)

National Defence / Défense nationale

PLEASE RETURN THIS DOCUMENT TO THE FOLLOWING ADDRESS:

DIRECTOR
SCIENTIFIC INFORMATION SERVICES
NATIONAL DEFENCE
HEADQUARTERS
OTTAWA, ONT. - CANADA K1A 0K2

PRIÈRE DE RETOURNER CE DOCUMENT À L'ADRESSE SUIVANTE:

DIRECTEUR
SERVICES D'INFORMATION SCIENTIFIQUES
QUARTIER GÉNÉRAL
DE LA DÉFENSE NATIONALE
OTTAWA, ONT. - CANADA K1A 0K2